Optics Communications 475 (2020) 126193

Contents lists available at ScienceDirect

Optics Communications

journal homepage: www.elsevier.com/locate/optcom

Secrecy enhancement of RF backhaul system with parallel FSO communication link

Yun Ai [a,*], Aashish Mathur [b], Hongjiang Lei [c,d], Michael Cheffena [a], Imran Shafique Ansari [e]

[a] Faculty of Engineering, Norwegian University of Science and Technology (NTNU), 2815 Gjøvik, Norway
[b] Department of Electrical Engineering, Indian Institute of Technology Jodhpur, Jodhpur 342037, India
[c] Chongqing Key Laboratory of Mobile Communications Technology, Chongqing University of Posts and Telecommunications, Chongqing 400065, China
[d] Shannxi Key Laboratory of Information Communication Network and Security, Xi'an University of Posts and Telecommunications, Xi'an 710121, China
[e] James Watt School of Engineering, University of Glasgow, Glasgow G12 8QQ, United Kingdom

ARTICLE INFO

Keywords:
Physical layer security
5G backhaul
Free-space optical (FSO) communication
Radio frequency (RF) communication
Parallel links

ABSTRACT

This paper analyzes the physical layer secrecy (PLS) performance of a hybrid free space optical and radio frequency (FSO/RF) communication system under a modified selection combining scheme. The transmission scheme takes into account secrecy performance as well as diversity gain and ease of implementation. The effects of FSO link, namely the FSO atmospheric turbulence and the FSO receiver pointing error, are included in the analysis while the power amplifier (PA) inefficiency for the RF transmission is considered to have more realistic understandings on the system performance. The exact analytical expressions for the performance indicators including the average secrecy capacity (ASC) and secrecy outage probability (SOP) of the investigated mixed FSO/RF system are derived. The asymptotic SOP analysis reveals useful insights into the performance of the investigated mixed system. Analytical and simulation results are presented to evaluate the PLS performance of the proposed mixed system as well as to compare the performance of other hybrid systems with different setups.

1. Introduction

1.1. Research background

The growing demands for extremely high data rate in the next generation mobile systems (5G and beyond) require backhaul links with much higher capacity and reliability relative to previous systems (especially in the context of network densification that makes wired backhaul an expensive solution and of the fact that integrated access backhaul (IAB) solution is officially adopted in 5G standard of 3GPP recently) [1]. The conventional RF backhaul can be potentially limited by latency problem due to the limited throughput, but is advantageous of being insensitive to weather effects. The broadcasting nature of radio wave propagation also makes RF communication vulnerable to eavesdropping attack. On the other hand, FSO communication features high-rate and low latency transmission, but it is highly susceptible to the atmospheric conditions and adverse weather effects [2]. It is also well accepted by both academia and industry that the point-to-point propagation with extreme narrow divergence of FSO beam makes physical interception and eavesdropping extremely difficult and the chance of an attempted intercept being discovered extremely high, thus making FSO communication an inherently secure technology [3–6]. To combine the advantages of RF communication (in terms of its robustness to atmospheric and weather effects) and FSO communication (in terms of secure transmission with high data rate), the parallel setup of FSO and RF communication systems have been developed as a more reliable candidate solution for backhaul network as an integral part of 5G system as well as in many other applications. The parallel system uses both optical and radio links for information transmission and it can simply adjust the use of both links depending on the wireless interference levels and atmospheric conditions [1].

1.2. Literature review and motivations

Due to the great potential of parallel FSO/RF scheme in 5G backhaul network and many other applications, a number of research works have been conducted in the domain of performance analysis of such systems [6–12]. A hybrid radio/optical system with a new implementation of selection combining (SC) scheme was investigated in [6], where the same data is sent over both links concurrently. The work in [6] focused on the analysis of bit error rate (BER) and connection outage probability (COP). A switching-based parallel system was proposed in [7], where the BER and COP performance were analyzed. The COP of a hybrid system with adaptive combining was studied in [8], where the maximal ratio combining (MRC) is applied when the link quality of

* Corresponding author.
E-mail address: yun.ai@ntnu.no (Y. Ai).

https://doi.org/10.1016/j.optcom.2020.126193
Received 11 May 2020; Received in revised form 13 June 2020; Accepted 15 June 2020
Available online 20 June 2020

the optical channel plunges under some predefined level. The BER and COP of a hybrid system were computed in [9] by including various FSO impairments (i.e., atmospheric turbulence and FSO receiver misalignment). In [10], the effect of different power allocation schemes on BER of a hybrid system was studied and a suboptimal allocation strategy was proposed. The throughput of a relaying system was investigated in [11], where two hops employ respectively the RF and parallel FSO/RF techniques. The impact of automatic repeat request (ARQ) schemes on the parallel radio/optical configuration was investigated in [12], which showed significant performance improvement with the parallel implementation of both links compared to using only one of the links. It is clear from [6–12] and the references therein that most existing work on the parallel FSO/RF system has focused on the BER and COP performance. A thorough search in open literature confirms that the existing works on the physical layer security (PLS) of hybrid FSO and RF systems are confined to the cascaded dual-hop FSO–RF systems [5,13–18], and the PLS of parallel FSO/RF configuration is not yet explored despite the great potential of the system in various applications.

The PLS has been widely viewed as a complementary instrument to conventional cryptographic technique to significantly enhance the security of communication in 5G and beyond [19]. It was demonstrated in the pioneering work of Information Theory by Shannon and Bloch, etc., that secure communication is feasible by utilizing the characteristics of the physical channel (e.g., fading, noise, interference, etc.) [20]. Therefore, the latest advancements in PLS [5,13–18] coupled with the great potential of parallel FSO/RF system in various applications have motivated us to analyze the PLS performance of such a system configuration in this research. The choice of SC scheme of the parallel FSO/RF setup in this research paper is justified by the trade-off between connection, secrecy, and complexity. While MRC diversity gain can be obtained while both the FSO and RF transmitters send the confidential information, this approach is also subject to the continuous eavesdropping from the eavesdropper. Additionally, the FSO channel coherence time is normally very small (around $0.1\sim1$ percent of RF channel coherence time), which poses challenges for the channel estimation required under MRC scheme [10].

Further, to obtain realistic insights into the investigated parallel system performance, we take the practical link impairments into consideration. More specifically, the effects of FSO link turbulence and FSO receiver pointing error are included in the analysis of the FSO subsystem [5]. For the RF subsystem, the inefficiency of the power amplifier (PA) is the major hardware constraint limiting the performance [21], which is also included in the analysis. It must be noted that the conducted secrecy analysis in this paper significantly differs from those conducted in [5,13–18], where the FSO link is only part of cascaded FSO–RF dual-hop relay system. The differences in the system structures of parallel FSO/RF and cascaded FSO–RF networks make them have different advantages and also different methods of analysis. The cascaded dual-hop FSO–RF relay system is advantageous in terms of extending the connection distance [5]. However, the nature of relaying in the dual-hop FSO–RF system indicates that the end-to-end performance can be hindered by either link. The parallel FSO/RF system has the benefits of high data transmission rate enabled by FSO link. At the same time, the additional RF link in the parallel setup makes the system more robust to the adverse weather effects. Thus, contrary to the dual-hop relaying system, the parallel FSO/RF system would be preferred when the communication link requires high-data rate and extremely reliable communication as in the case of backhaul transmission [1].

The major contributions of the paper are the following:

(i). Despite great potentials of parallel FSO/RF system as a strong candidate for the backhaul network of future networks as well as in many other applications, the PLS performance of the parallel radio/optical system has not yet been analyzed in open literature to the authors' best knowledge. Thus, we study the secrecy performance of such a setup in this paper.

(ii). To make the conducted analysis more practical, the main impairments or characteristics of the FSO and RF communications (e.g., PA inefficiency for RF sub-system, and atmospheric turbulence, misalignment, detection types for FSO sub-system) are also taken into account.

(iii). We derive the exact analytical expressions for the secrecy outage probability (SOP), probability of strictly positive secrecy capacity (SPSC), and the average secrecy capacity (ASC) in this work contrary to previous PLS works on FSO communication systems [13–15], where only the lower bounds on SOP were computed.

(iv). The asymptotic SOP analysis is performed and the corresponding diversity orders under various conditions are obtained to reveal some useful insights into the PLS performance of the investigated parallel system.

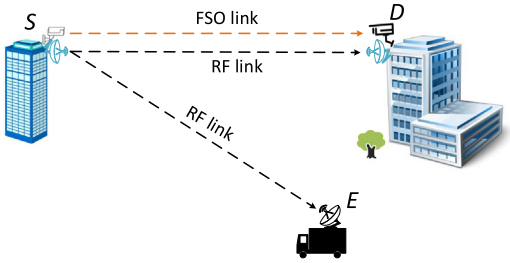

Fig. 1. Investigated secrecy problem of the parallel FSO/RF configuration.

1.3. Organization of the paper

The remainder of this work is structured as follows. The investigated SC-based parallel FSO/RF setup is introduced in Section 2 followed by the derivation of ASC in Section 3. In Section 4, the SOP analysis and asymptotic SOP analysis is conducted. The simulation and analytical results with the corresponding discussions are presented in Section 5. Section 6 briefly highlights the conclusions of this research.

1.4. Notations

The following mathematical notations are applied throughout the paper. $\Gamma(\cdot)$ and $\hat{\Gamma}(\cdot,\cdot)$ are, respectively, Gamma function [22, Eq. (8.31)] and lower incomplete Gamma function [22, Eq. (8.35)], $G_{p,q}^{m,n}(x|\cdot)$ defines the Meijer G-function [22, Eq. (9.343)], $\Delta(i,j) = \frac{j}{i}, \frac{j+1}{i}, \ldots, \frac{j+i-1}{i}$ consisting of i terms, $\max\{a,b\}$ represents the maximum value of a and b. $E\{\cdot\}$ represents the expectation operator.

2. Investigated system and channels models

2.1. Investigated system

The PLS of the investigated SC-based parallel FSO/RF setup in this research work is illustrated as in Fig. 1, where the best link of the RF and FSO links is used for information transmission while the other link is idle. The transmitter (S) of the parallel SC-based optical/radio system transmits confidential messages to a desired receiver (D). Additionally, an eavesdropper (E) tries to intercept the confidential messages from S. Due to the good directivity of FSO signal and broadcasting nature of RF signal, the node E can only eavesdrop the information when the radio part of the parallel configuration is transmitting the confidential information.

2.2. Channel models

The FSO link turbulence is statistically characterized by the Gamma–Gamma distribution [2] whereas the fading in RF channels is characterized by the Nakagami-m distribution [23]. The choice of Nakagami model to describe the RF fading is justified as follows. On the one hand, the simple formed model fits a number of propagation scenarios well [24]. On the other hand, the model can degrade to or approach other widely used model well (e.g., Rayleigh, Rician, lognormal, Weibull, etc.) [25]. It is further assumed that the phasefront of the FSO signal is perfectly estimated and compensated at the FSO receiver, which enables ideal coherent detection at the receiver [14].

2.2.1. FSO communications

By assuming the fading on the FSO link to follow Gamma–Gamma turbulence model and taking into account of the FSO pointing errors caused by jitter, the probability distribution function (PDF) $f_{\gamma_{FSO}}(\cdot)$ of instantaneous SNR γ_{FSO} is [2]

$$f_{\gamma_{FSO}}(x) = \frac{c^2}{t\,\Gamma(a)\Gamma(b)x} \cdot G_{1,3}^{3,0}\left(hab\left(\frac{x}{\mu_t}\right)^{\frac{1}{t}} \middle| \begin{matrix} c^2+1 \\ c^2, a, b \end{matrix} \right). \tag{1}$$

In (1), a and b imply the severity of fading resulting from turbulent flow [26], μ_t is the link's SNR with heterodyne detection (HD) for $t = 1$ or with intensity modulation under direct detection (IM/DD) for $t = 2$ being used at receiver [2], c^2 denotes the ratio between squared radius of equivalent ray and variance of the FSO receiver jitting movement [15], and $h = \frac{c^2}{c^2+1}$. Hereinafter, we apply the following simplifications: $\mathcal{A} = \frac{c^2}{t\Gamma(a)\Gamma(b)}, \mathcal{B} = hab\mu_t^{-\frac{1}{t}}$. Therefore, the PDF $f_{\gamma_{FSO}}(x)$ can be alternatively expressed as: $f_{\gamma_{FSO}}(x) = \frac{\mathcal{A}}{x} \cdot G_{1,3}^{3,0}\left(\mathcal{B}x^{\frac{1}{t}} \middle| \begin{matrix} c^2+1 \\ c^2, a, b \end{matrix} \right)$.

From (1), the cumulative distribution function (CDF) $F_{\gamma_{FSO}}(\cdot)$ of γ_{FSO} is expressed as [27]

$$F_{\gamma_{FSO}}(x) = \frac{c^2\, t^{a+b-2}}{\Gamma(a)\Gamma(b)(2\pi)^{t-1}} \cdot G_{t+1,3t+1}^{3t,1}\left(\frac{(hab)^t}{t^{2t}\mu_t} x \middle| \begin{matrix} 1, \Delta(t,c^2+1) \\ \Delta(t,c^2), \Delta(t,a), \Delta(t,b), 0 \end{matrix} \right). \tag{2}$$

For simplicity, the following notations will be used in the rest of the paper: $C = \frac{c^2\, t^{a+b-2}}{(2\pi)^{t-1}\Gamma(a)\Gamma(b)}, D = \frac{(hab)^t}{\mu_t\, t^{2t}}, \Lambda_1 = 1, \Delta(t, c^2+1), \Lambda_2 = \Delta(t,c^2), \Delta(t,a), \Delta(t,b), 0$. As a result, the CDF $F_{\gamma_{FSO}}(x)$ is expressed by $F_{\gamma_{FSO}}(x) = C \cdot G_{t+1,3t+1}^{3t,1}\left(Dx \middle| \begin{matrix} \Lambda_1 \\ \Lambda_2 \end{matrix} \right)$.

Remark 1. It is noteworthy that another widely used model to describe the FSO turbulence is the Málaga model that was proposed in [28]. By observing the distribution functions of the Gamma–Gamma and Málaga models, it is evident that they exhibit similar form. Thus, the analytical method applied in this work can be straightforwardly expanded to the case assuming the Málaga fading for the FSO turbulence. ■

2.2.2. RF communications

With the Nakagami fading of the RF channels, the PDF $f_{\gamma_{RF,X}}(\cdot)$ and CDF $F_{\gamma_{RF,X}}(\cdot)$ of the instantaneous SNR $\gamma_{RF,X}$ for the RF link between the transmitter S and receiver X are given by [29,30]

$$f_{\gamma_{RF,X}}(x) = \left(\frac{m_X}{\overline{\gamma}_{RF,X}}\right)^{m_X} \cdot \frac{x^{m_X-1}}{\Gamma(m_X)} \cdot \exp\left(-\frac{m_X \cdot x}{\overline{\gamma}_{RF,X}}\right), \tag{3}$$

$$F_{\gamma_{RF,X}}(x) = \frac{1}{\Gamma(m_X)} \cdot \hat{\Gamma}\left(m_X, \frac{m_X \cdot x}{\overline{\gamma}_{RF,X}}\right), \tag{4}$$

where $\overline{\gamma}_{RF,X} = P_{RF} \cdot \Omega_X$ is average SNR between transmitter S and receiver X, P_{RF} is the transmit power, m_X and Ω_X respectively are shape factor and average channel gain of corresponding Nakagami fading link.

To account for the effect of non-ideal PA in the RF link, we utilize the following relationship for the PA efficiency [21]:

$$P_{RF} = \left[\frac{\zeta \cdot P_{RF}^{cons}}{(P_{RF}^{max})^{\psi}}\right]^{\frac{1}{1-\psi}}, \tag{5}$$

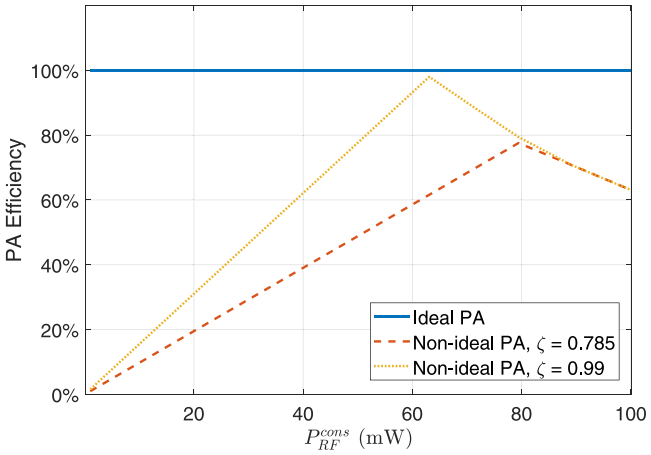

Fig. 2. PA efficiency v.s. P_{RF}^{cons} for PAs with varying levels of PA efficiency.

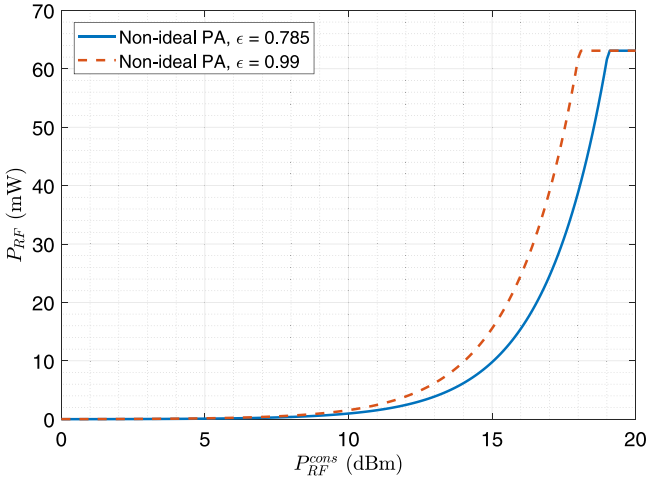

Fig. 3. Output power of imperfect PA v.s. P_{RF}^{cons}.

where P_{RF}, P_{RF}^{max}, and P_{RF}^{cons} respectively denote amplifier's output power, output power limit, and input power of amplifier; the parameter ζ represents the amplifier efficiency limit that is reached when $P_{RF} = P_{RF}^{max}$, and the parameter ψ is related to the class of the PA. Both parameters ζ and ψ are within the range of 0 and 1. The PA efficiency model in (5) has been widely used in the analysis that includes non-ideal amplifier [31–33]. Additionally, the accuracy of the model on different classes of amplifiers has been verified by efficiency measurements conducted in the microwave electronics lab of Chalmers University of Technology, Sweden [34]. The relationship between the consumed power P_{RF}^{cons} and the PA efficiency defined as $\frac{P_{RF}}{P_{RF}^{cons}}$ is illustrated in Fig. 2 for different classes of PAs, where $P_{max} = 18$ mW and $\psi = 0.5$. The relationship between the output power P_{RF} and consumed power P_{RF}^{cons} for imperfect PAs is shown in Fig. 3. It can be seen that the output power of PA does not improve much as the power P_{RF}^{cons} is small due to low efficiency as well as low power.

Remark 2. As illustrated in Fig. 2, the efficiency of imperfect PAs improves as the input power increases until some saturation point is reached. With other factors being the same, the saturation point for the PA with larger maximum efficiency is found to be lower than that with lower maximum efficiency. ■

2.3. Selection combining scheme

With the receiver employing the SC scheme, the equivalent SNR γ_{sc} of the parallel setup relies upon the SNRs of optical communication channel γ_{FSO} and legitimate RF communication link $\gamma_{RF,D}$, i.e. [35, Chpt. 9.7],

$$\gamma_{sc} = \max\{\gamma_{FSO}, \gamma_{RF,D}\}. \tag{6}$$

The CDF $F_{\gamma_{sc}}(\cdot)$ of the SNR γ_{sc} can be obtained directly as

$$\begin{aligned} F_{\gamma_{sc}}(x) &= \Pr(\gamma_{sc} < x) = \Pr(\gamma_{FSO} < x) \cdot \Pr(\gamma_{RF,D} < x) = F_{\gamma_{FSO}}(x) \cdot F_{\gamma_{RF,D}}(x) \\ &= \mathcal{C} \cdot G_{t+1,3t+1}^{3t,1}\left(\mathcal{D}x \middle| \begin{matrix} \Lambda_1 \\ \Lambda_2 \end{matrix} \right) \cdot \frac{1}{\Gamma(m_D)} \cdot \hat{\Gamma}\left(m_D, \frac{m_D \cdot x}{\overline{\gamma}_{RF,D}} \right). \end{aligned} \tag{7}$$

Then, the PDF $f_{\gamma_{sc}}(\cdot)$ of the SNR γ_{sc} can be obtained from the differentiation of the CDF given in (7) and is obtained as

$$\begin{aligned} f_{\gamma_{sc}}(x) &= F_{\gamma_{FSO}}(x) \cdot f_{\gamma_{RF,D}}(x) + f_{\gamma_{FSO}}(x) \cdot F_{\gamma_{RF,D}}(x) \\ &= \mathcal{C} \cdot G_{t+1,3t+1}^{3t,1}\left(\mathcal{D}x \middle| \begin{matrix} \Lambda_1 \\ \Lambda_2 \end{matrix} \right) \cdot \left(\frac{m_D}{\overline{\gamma}_{RF,D}} \right)^{m_D} \cdot \frac{x^{m_D-1}}{\Gamma(m_D)} \cdot \exp\left(-\frac{m_D \cdot x}{\overline{\gamma}_{RF,D}} \right) \\ &\quad + \frac{\mathcal{A}}{x} \cdot G_{1,3}^{3,0}\left(\mathcal{B}x^{\frac{1}{t}} \middle| \begin{matrix} c^2+1 \\ c^2, a, b \end{matrix} \right) \cdot \frac{1}{\Gamma(m_D)} \cdot \hat{\Gamma}\left(m_D, \frac{m_D \cdot x}{\overline{\gamma}_{RF,D}} \right). \end{aligned} \tag{8}$$

3. Analysis of average secrecy rate

By definition, the secrecy rate that indicates the maximum achievable perfect secrecy rate in Wyner's wiretap model is [36]

$$C_s(\gamma_{sc}, \gamma_{RF,E}) = \max\left\{ 0, \ln\left(\frac{\gamma_{sc}+1}{\gamma_{RF,E}+1} \right) \right\}, \tag{9}$$

where $\gamma_{RF,E}$ and γ_{sc} respectively denote instantaneous SNRs of the radio wiretap link and legitimate link that consists of the parallel radio and optical channels.

In case of active eavesdropping scenario, the source node can adapt the achievable secrecy rate accordingly and the ASC is the secrecy performance metric that is of central importance in this case. From instantaneous secrecy capacity, the ASC $\overline{C}_s$ is mathematically expressed as [37]

$$\overline{C}_s = E\left[C_s(\gamma_{sc}, \gamma_{RF,E}) \right] = E\left\{ \max\left\{ 0, \ln\left(\frac{\gamma_{sc}+1}{\gamma_{RF,E}+1} \right) \right\} \right\}. \tag{10}$$

Noticing that the FSO communication is secure while RF transmission is subject to eavesdropping, the ASC of investigated parallel setup under proposed combining scheme is further given by

$$\begin{aligned} \overline{C}_s &= \underbrace{E\{\ln(1+\gamma_{sc})\}}_{\overline{C}_1} \cdot \underbrace{\Pr\left[\gamma_{sc} = \gamma_{FSO}\right]}_{P_1} + \underbrace{E\left\{ \max\left\{ 0, \ln\left(\frac{\gamma_{sc}+1}{\gamma_{RF,E}+1} \right) \right\} \right\}}_{\overline{C}_2} \\ &\quad \underbrace{\cdot \Pr\left[\gamma_{sc} = \gamma_{RF,D}\right]}_{1-P_1} \\ &= \overline{C}_1 \cdot P_1 + \overline{C}_2 - \overline{C}_2 \cdot P_1. \end{aligned} \tag{11}$$

Evaluation of P_1: The probability P_1 indicates the scenario, where the optical link's SNR is larger than RF link's. We can solve the probability P_1 as

$$\begin{aligned} P_1 &= \Pr\left[\gamma_{sc} = \gamma_{FSO}\right] = \Pr\left[\gamma_{FSO} > \gamma_{RF,D}\right] \\ &= \int_0^\infty \int_0^y f_{\gamma_{RF,D}}(x) \cdot f_{\gamma_{FSO}}(y)\, dx dy = 1 - \int_0^\infty f_{\gamma_{RF,D}}(y) \cdot F_{\gamma_{FSO}}(y)\, dy. \end{aligned} \tag{12}$$

Substituting (2) and (3) into (12) and rewriting the exponential term with the G-function [38, Eq. (8.4)] and further employing property [38, Eq. (2.24)], the exact expression of the probability P_1 can be obtained as follows:

$$\begin{aligned} P_1 &= 1 - \frac{\mathcal{C}}{\Gamma(m_D)} \cdot \left(\frac{m_D}{\overline{\gamma}_{RF,D}} \right)^{m_D} \int_0^\infty y^{m_D-1} \cdot G_{0,1}^{1,0}\left(\frac{m_D y}{\overline{\gamma}_{RF,D}} \middle| \begin{matrix} - \\ 0 \end{matrix} \right) \\ &\quad \cdot G_{t+1,3t+1}^{3t,1}\left(\mathcal{D}y \middle| \begin{matrix} \Lambda_1 \\ \Lambda_2 \end{matrix} \right) dy \\ &= 1 - \frac{\mathcal{C}}{\Gamma(m_D)} \cdot G_{t+2,3t+1}^{3t,2}\left(\frac{\mathcal{D}\overline{\gamma}_{RF,D}}{m_D} \middle| \begin{matrix} 1, 1-m_D, \Delta(t, c^2+1) \\ \Lambda_2 \end{matrix} \right). \end{aligned} \tag{13}$$

Evaluation of $\overline{C}_1$: By definition, the average capacity $\overline{C}_1 = E\{\ln(\gamma_{sc}+1)\}$ can be obtained as follows:

$$\begin{aligned} \overline{C}_1 &= \int_0^\infty F_{\gamma_{FSO}}(x) \cdot f_{\gamma_{RF,D}}(x) \cdot \ln(x+1)\, dx \\ &\quad + \int_0^\infty f_{\gamma_{FSO}}(x) \cdot F_{\gamma_{RF,D}}(x) \cdot \ln(x+1)\, dx \\ &= C_{1a} + C_{1b}, \end{aligned} \tag{14}$$

where C_{1a} and C_{1b} can be further expressed as

$$\begin{aligned} C_{1a} &= \frac{m_D^{m_D} \cdot \mathcal{C}}{\Gamma(m_D) \cdot \overline{\gamma}_{RF,D}^{m_D}} \cdot \int_0^\infty x^{m_D-1} \cdot \ln(x+1) \\ &\quad \cdot G_{t+1,3t+1}^{3t,1}\left(\mathcal{D}x \middle| \begin{matrix} \Lambda_1 \\ \Lambda_2 \end{matrix} \right) \cdot \exp\left(-\frac{m_D \cdot x}{\overline{\gamma}_{RF,D}} \right) dx, \end{aligned} \tag{15}$$

$$C_{1b} = \frac{\mathcal{A}}{\Gamma(m_D)} \cdot \int_0^\infty \frac{1}{x} \cdot \ln(x+1) \cdot G_{1,3}^{3,0}\left(\mathcal{B}x^{\frac{1}{t}} \middle| \begin{matrix} c^2+1 \\ c^2, a, b \end{matrix} \right) \cdot \hat{\Gamma}\left(m_D, \frac{m_D \cdot x}{\overline{\gamma}_{RF,D}} \right) dx. \tag{16}$$

To solve the integrals C_{1a} and C_{1b}, we utilize the following transformations involving the Meijer G-function [38, Chpt. 8.4], [39, Eq. (8)]:

$$\ln(x+1) = G_{2,2}^{1,2}\left(x \middle| \begin{matrix} 1,1 \\ 1,0 \end{matrix} \right), \tag{17a}$$

$$\exp(-ax) = G_{0,1}^{1,0}\left(ax \middle| \begin{matrix} - \\ 0 \end{matrix} \right), \tag{17b}$$

$$\hat{\Gamma}(a, x) = G_{1,2}^{1,1}\left(x \middle| \begin{matrix} 1 \\ a,0 \end{matrix} \right), \tag{17c}$$

and the following relationship that is obtained by making use of the identity [40, Eq. (2.3)] and the relationship [38, Eq. (8.3.2.21)]:

$$\begin{aligned} &\int_0^\infty x^{\lambda-1} \cdot G_{p,q}^{m,0}\left(\eta x \middle| \begin{matrix} \mathbf{a}_p \\ \mathbf{b}_q \end{matrix} \right) \cdot G_{p_2,q_2}^{m_2,n_2}\left(\theta x^h \middle| \begin{matrix} \mathbf{c}_{p_2} \\ \mathbf{d}_{q_2} \end{matrix} \right) \cdot G_{p_3,q_3}^{m_3,n_3}\left(\delta x^k \middle| \begin{matrix} \mathbf{e}_{p_3} \\ \mathbf{f}_{q_3} \end{matrix} \right) dx = \eta^{-\lambda} \\ &\quad \cdot H_{q,p:p_2,q_2:p_3,q_3}^{0,m:m_2,n_2:m_3,n_3}\left(\begin{matrix} (1-\mathbf{b}_q-\lambda; h, k) \\ (1-\mathbf{a}_p-\lambda; h, k) \end{matrix} \middle| \begin{matrix} (\mathbf{c}_{p_2}, 1) \\ (\mathbf{d}_{q_2}, 1) \end{matrix} \middle| \begin{matrix} (\mathbf{e}_{p_3}, 1) \\ (\mathbf{f}_{q_3}, 1) \end{matrix} \middle| \begin{matrix} \frac{\theta}{\eta^h}, \frac{\delta}{\eta^k} \end{matrix} \right). \end{aligned} \tag{18}$$

In (18), $H_{p,q:u,v:e,f}^{m,n:s,t:i,j}(\cdot)$ represents the extended generalized bivariate Fox H-function (EGBFHF) [40]. This function can be conveniently evaluated using mathematical softwares such as Mathematica [41, Table I] and Matlab [42, Appx A].

Expressing the relevant functions in (15) and (16) into Meijer G-function using the above equalities in (17), we can solve the resultant integrals with the aid of (18) as given in Box I.

Evaluation of $\overline{C}_2$: The average capacity $\overline{C}_2$ can be expressed as

$$\begin{aligned} \overline{C}_2 &= \int_0^\infty \int_0^\infty f_{\gamma_{sc}}(\gamma_{sc}) \cdot f_{\gamma_{RF,E}}(\gamma_{RF,E}) \cdot C_s(\gamma_{sc}, \gamma_{RF,E})\, d\gamma_{sc} d\gamma_{RF,E} \\ &= \int_0^\infty \frac{1}{x+1} \cdot \left[1 - F_{\gamma_{sc}}(x) \right] \cdot F_{\gamma_{RF,E}}(x)\, dx = C_{2a} - C_{2b}, \end{aligned} \tag{21}$$

where

$$C_{2a} = \frac{1}{\Gamma(m_E)} \cdot \int_0^\infty \frac{1}{x+1} \cdot \hat{\Gamma}\left(m_E, \frac{m_E \cdot x}{\overline{\gamma}_{RF,E}} \right) dx, \tag{22}$$

$$\begin{aligned} C_{2b} &= \frac{\mathcal{C}}{\Gamma(m_D)\Gamma(m_E)} \cdot \int_0^\infty \frac{1}{x+1} \cdot G_{t+1,3t+1}^{3t,1}\left(\mathcal{D}x \middle| \begin{matrix} \Lambda_1 \\ \Lambda_2 \end{matrix} \right) \\ &\quad \cdot \hat{\Gamma}\left(m_E, \frac{m_E \cdot x}{\overline{\gamma}_{RF,E}} \right) \cdot \hat{\Gamma}\left(m_D, \frac{m_D \cdot x}{\overline{\gamma}_{RF,D}} \right) dx. \end{aligned} \tag{23}$$

We first solve the integral C_{2a} by expressing the lower incomplete Gamma function with the G-function using (17) and utilizing the identity $\frac{1}{x+1} = G_{1,1}^{1,1}\left(x \middle| \begin{matrix} 0 \\ 0 \end{matrix} \right)$ [43]; then with the aid of [44, Eq. (07.34.21.0011.01)], C_{2a} is obtained as

$$C_{2a} = \frac{1}{\Gamma(m_E)} \cdot G_{2,3}^{2,2}\left(\frac{m_E}{\overline{\gamma}_{RF,E}} \middle| \begin{matrix} 1,0 \\ m_E, 0, 0 \end{matrix} \right). \tag{24}$$

$$C_{1a} = \frac{\mathcal{C}}{\Gamma(m_D)} \cdot H^{0,1:1,2:3t,1}_{1,0:2,2:t+1,3t+1}\left(\begin{matrix} (1-m_D;1,1) \\ - \end{matrix} \middle| \begin{matrix} (1,1),(1,1) \\ (1,1),(0,1) \end{matrix} \middle| \begin{matrix} (\Lambda_1,1) \\ (\Lambda_2,1) \end{matrix} \middle| \begin{matrix} \frac{\overline{\gamma}_{RF,D}}{m_D}, \frac{\mathcal{D}\overline{\gamma}_{RF,D}}{m_D} \end{matrix} \right), \tag{19}$$

$$C_{1b} = \frac{\mathcal{A}t}{\Gamma(m_D)} \cdot H^{0,3:1,2:1,1}_{3,1:2,2:1,2}\left(\begin{matrix} (1-c^2;t,t),(1-a;t,t),(1-b;t,t) \\ (-c^2;t,t) \end{matrix} \middle| \begin{matrix} (1,1),(1,1) \\ (1,1),(0,1) \end{matrix} \middle| \begin{matrix} (1,1) \\ (m_D,1),(0,1) \end{matrix} \middle| \begin{matrix} \frac{1}{\mathcal{B}^t}, \frac{m_D}{\overline{\gamma}_{RF,D}\mathcal{B}^t} \end{matrix} \right). \tag{20}$$

Box I.

To solve the single integral C_{2b}, we first express the lower incomplete Gamma functions in (23) in series [15, Eq. (2)], convert to relevant terms in Meijer G-function, and then solve the resultant integrals with the identity (18) to obtain

$$C_{2b} = \mathcal{C} \cdot \left[G^{3t+1,2}_{t+2,3t+3}\left(\mathcal{D} \middle| \begin{matrix} 0,\Lambda_1 \\ 0,\Lambda_2 \end{matrix} \right) - \sum_{\omega=0}^{m_D-1} \frac{\overline{\gamma}_{RF,D}}{m_D \cdot \omega!} \cdot \mathcal{H}_1 - \sum_{\nu=0}^{m_E-1} \frac{\overline{\gamma}_{RF,E}}{m_E \cdot \nu!} \cdot \mathcal{H}_2 + \sum_{\omega=0}^{m_D-1} \sum_{\nu=0}^{m_E-1} \frac{m_D^{\omega} \cdot m_E^{\nu}}{\overline{\gamma}_{RF,D}^{\omega} \cdot \overline{\gamma}_{RF,E}^{\nu} \cdot \omega! \cdot \nu!} \cdot \left(\frac{m_D}{\overline{\gamma}_{RF,D}} + \frac{m_E}{\overline{\gamma}_{RF,E}} \right)^{-(\omega+\nu+1)} \cdot \mathcal{H}_3 \right], \tag{25}$$

where

$$\mathcal{H}_1 = H^{0,1:1,1:3t,1}_{1,0:1,1:t+1,3t+1}\left(\begin{matrix} (-\omega;1,1) \\ - \end{matrix} \middle| \begin{matrix} (0,1) \\ (0,1) \end{matrix} \middle| \begin{matrix} (\Lambda_1,1) \\ (\Lambda_2,1) \end{matrix} \middle| \begin{matrix} \frac{\overline{\gamma}_{RF,D}}{m_D}, \frac{\mathcal{D}\overline{\gamma}_{RF,D}}{m_D} \end{matrix} \right), \tag{26a}$$

$$\mathcal{H}_2 = H^{0,1:1,1:3t,1}_{1,0:1,1:t+1,3t+1}\left(\begin{matrix} (-\nu;1,1) \\ - \end{matrix} \middle| \begin{matrix} (0,1) \\ (0,1) \end{matrix} \middle| \begin{matrix} (\Lambda_1,1) \\ (\Lambda_2,1) \end{matrix} \middle| \begin{matrix} \frac{\overline{\gamma}_{RF,E}}{m_E}, \frac{\mathcal{D}\overline{\gamma}_{RF,E}}{m_E} \end{matrix} \right), \tag{26b}$$

$$\mathcal{H}_3 = H^{0,1:1,1:3t,1}_{1,0:1,1:t+1,3t+1}\left(\begin{matrix} (-(\omega+\nu);1,1) \\ - \end{matrix} \middle| \begin{matrix} (0,1) \\ (0,1) \end{matrix} \middle| \begin{matrix} (\Lambda_1,1) \\ (\Lambda_2,1) \end{matrix} \middle| \begin{matrix} \frac{\overline{\gamma}_{RF,D}\mathcal{D}\overline{\gamma}_{RF,E}}{m_E\overline{\gamma}_{RF,D}+m_D\overline{\gamma}_{RF,E}}, \frac{\mathcal{D}\overline{\gamma}_{RF,D}\mathcal{D}\overline{\gamma}_{RF,E}}{m_E\overline{\gamma}_{RF,D}+m_D\overline{\gamma}_{RF,E}} \end{matrix} \right). \tag{26c}$$

Finally, substituting the expressions of P_1, $\overline{C}_1$, and $\overline{C}_2$ into (11), the exact closed-form solution for ASC of the investigated system is obtained.

4. Analysis of secrecy outage performance

4.1. Connection outage probability analysis

Before analyzing the SOP, we first evaluate the COP of the investigated system. The COP implies the scenario that the legitimate receiver is unable to decode the sent information correctly. This occurs while γ_{sc} is smaller than a given threshold γ_{th} [45]. Therefore, the investigated COP can be directly derived from CDF of γ_{sc} as follows:

$$COP = \Pr\left[\gamma_{sc} \le \gamma_{th}\right] = \mathcal{C} \cdot G^{3t,1}_{t+1,3t+1}\left(\mathcal{D} \cdot \gamma_{th} \middle| \begin{matrix} \Lambda_1 \\ \Lambda_2 \end{matrix} \right) \cdot \frac{1}{\Gamma(m_D)} \cdot \hat{\Gamma}\left(m_D, \frac{m_D \cdot \gamma_{th}}{\overline{\gamma}_{RF,D}} \right). \tag{27}$$

4.2. Secrecy outage probability analysis

In the passive eavesdropping case, the transmitter resorts to encode and transmit the confidential information into codewords with some constant rate R_s. If $C_s(\gamma_{sc}, \gamma_{RF,E}) \ge R_s$, perfectly secure information transmission can be achieved, otherwise information secrecy is subject to be undermined [46]. Under such scenario, SOP is the most essential performance indicator, which describes the likelihood the secrecy capacity is below some threshold [47]. The SOP is mathematically expressed as [47]

$$SOP = \Pr\left[C_s(\gamma_{sc}, \gamma_{RF,E}) \le R_s\right] = \Pr\left[\gamma_{sc} \le \Theta\gamma_{RF,E} + \Theta - 1\right], \tag{28}$$

where $\Theta = \exp(R_s) \ge 1$.

Again, noticing that the eavesdropper can only eavesdrop via the RF link, the SOP of the parallel FSO/RF setup under investigation is further written as

$$\begin{aligned} SOP &= \underbrace{\Pr\left[\ln(1+\gamma_{sc}) < R_s\right]}_{P_0} \cdot \underbrace{\Pr\left[\gamma_{sc} = \gamma_{FSO}\right]}_{P_1} + \underbrace{\Pr\left[\gamma_{sc} \le \Theta\gamma_{RF,E} + \Theta - 1\right]}_{P_2} \\ &\quad \cdot \underbrace{\Pr\left[\gamma_{sc} = \gamma_{RF,D}\right]}_{1-P_1} \\ &= P_0 \cdot P_1 + P_2 - P_1 \cdot P_2, \end{aligned} \tag{29}$$

where the probability P_1 has already been solved in (12)–(13).

Evaluation of P_0: It is obvious that when the capacity of the eavesdropping link is zero, the SOP of the investigated system equals the COP. Hence, P_0 is solved as

$$P_0 = \mathcal{C} \cdot G^{3t,1}_{t+1,3t+1}\left(\mathcal{D} \cdot (\Theta - 1) \middle| \begin{matrix} \Lambda_1 \\ \Lambda_2 \end{matrix} \right) \cdot \frac{1}{\Gamma(m_D)} \cdot \hat{\Gamma}\left(m_D, \frac{m_D \cdot (\Theta - 1)}{\overline{\gamma}_{RF,D}} \right). \tag{30}$$

Evaluation of P_2: The probability P_2 is the SOP when the eavesdropper's link has nonzero channel capacity. The probability P_2 can be written as follows:

$$\begin{aligned} P_2 &= \Pr\left[\gamma_{sc} \le \Theta\gamma_{RF,E} + \Theta - 1\right] = \int_0^{\infty} \int_0^{(1+x)\Theta-1} f_{\gamma_{RF,E}}(x) \cdot f_{\gamma_{sc}}(y)\, dy dx \\ &= \int_0^{\infty} f_{\gamma_{RF,E}}(x) \cdot F_{\gamma_{sc}}((1+x)\Theta - 1)\, dx. \end{aligned} \tag{31}$$

Substituting (3) and (7) into (31), P_2 can be further expressed as

$$\begin{aligned} P_2 &= \frac{\mathcal{C}}{\Gamma(m_D)\Gamma(m_E)} \cdot \left(\frac{m_E}{\overline{\gamma}_{RF,E}} \right)^{m_E} \cdot \int_0^{\infty} x^{m_E-1} \cdot \exp\left(-\frac{m_E \cdot x}{\overline{\gamma}_{RF,E}} \right) \\ &\quad \cdot G^{3t,1}_{t+1,3t+1}\left(\mathcal{D} \cdot [(1+x) \cdot \Theta - 1] \middle| \begin{matrix} \Lambda_1 \\ \Lambda_2 \end{matrix} \right) \\ &\quad \cdot \hat{\Gamma}\left(m_D, \frac{m_D \cdot [(1+x) \cdot \Theta - 1]}{\overline{\gamma}_{RF,D}} \right) dx. \end{aligned} \tag{32}$$

The single integral in (32) is solved by using the transformation: $x = \frac{y+1}{\Theta} - 1$ and then writing the resultant polynomial in series, $[(1-\Theta)+y]^{m_E-1} = \sum_{k=0}^{m_E-1} \binom{m_E-1}{k} (1-\Theta)^{m_E-1-k} \cdot y^k$ to obtain

$$\begin{aligned} P_2 &= \frac{\mathcal{C} \cdot \Theta^{-m_E}}{\Gamma(m_D)\Gamma(m_E)} \cdot \left(\frac{m_E}{\overline{\gamma}_{RF,E}} \right)^{m_E} \cdot \exp\left(-\frac{m_E \cdot (1-\Theta)}{\overline{\gamma}_{RF,E} \cdot \Theta} \right) \cdot \sum_{k=0}^{m_E-1} \binom{m_E-1}{k} \\ &\quad \cdot (1-\Theta)^{m_E-1-k} \cdot \left[\mathcal{I}_a + \mathcal{I}_b \right], \end{aligned} \tag{33}$$

where

$$\mathcal{I}_a = \int_0^{\infty} y^k \cdot \exp\left(-\frac{m_E \cdot y}{\overline{\gamma}_{RF,E}} \right) \cdot G^{3t,1}_{t+1,3t+1}\left(\mathcal{D}y \middle| \begin{matrix} \Lambda_1 \\ \Lambda_2 \end{matrix} \right) \cdot \hat{\Gamma}\left(m_D, \frac{m_D \cdot y}{\overline{\gamma}_{RF,D}} \right) dy, \tag{34}$$

$$\mathcal{I}_b = \int_{\Theta-1}^{0} y^k \cdot \exp\left(-\frac{m_E \cdot y}{\overline{\gamma}_{RF,E}} \right) \cdot G^{3t,1}_{t+1,3t+1}\left(\mathcal{D}y \middle| \begin{matrix} \Lambda_1 \\ \Lambda_2 \end{matrix} \right) \cdot \hat{\Gamma}\left(m_D, \frac{m_D \cdot y}{\overline{\gamma}_{RF,D}} \right) dy. \tag{35}$$

Expressing the relevant functions in (34) into Meijer G-functions using identities in (17) and further using (18), we obtain

$$\mathcal{I}_a = \left(\frac{\overline{\gamma}_{RF,E}}{m_E} \right)^{k+1} \cdot H^{0,1:3t,1:1,1}_{1,0:t+1,3t+1:1,2}\left(\begin{matrix} (-k;1,1) \\ - \end{matrix} \middle| \begin{matrix} (\Lambda_1,1) \\ (\Lambda_2,1) \end{matrix} \middle| \begin{matrix} (1,1) \\ (m_D,1),(0,1) \end{matrix} \middle| \begin{matrix} \frac{\mathcal{D}\cdot\overline{\gamma}_{RF,E}}{m_E}, \frac{m_D\cdot\overline{\gamma}_{RF,E}}{m_E\cdot\overline{\gamma}_{RF,D}} \end{matrix} \right). \tag{36}$$

The term $\mathcal{I}_b$ can be efficiently evaluated by the definite integral in (35) using numerical softwares. Next, we compute the closed-form solution of $\mathcal{I}_b$ in following way: first we write the lower incomplete Gamma function in series with the help of [44, Eq. (06.06.06.0005.01)] and the exponential functions in terms of Taylor series [22, Eq. (1.211)], then solve the resultant integral using the antiderivative [44, Eq. (07.34.21.0003.01)], the probability $\mathcal{I}_b$ is solved as

$$\begin{aligned}\mathcal{I}_b =&\Gamma(m_D)\cdot\left[\sum_{s=0}^{\infty}\frac{1}{s!}\cdot\left(-\frac{m_E}{\overline{\gamma}_{RF,E}}\right)^s\cdot\int_{\Theta-1}^{0}y^{k+s}\cdot G_{t+1,3t+1}^{3t,1}\left(\mathcal{D}y\middle|\begin{matrix}\Lambda_1\\ \Lambda_2\end{matrix}\right)dy\right.\\ &-\sum_{q=0}^{m_D-1}\frac{1}{q!}\left(\frac{m_D}{\overline{\gamma}_{RF,D}}\right)^q\sum_{w=0}^{\infty}\frac{1}{w!}\left[-\left(\frac{m_E}{\overline{\gamma}_{RF,E}}+\frac{m_D}{\overline{\gamma}_{RF,D}}\right)\right]^w\cdot\int_{\Theta-1}^{0}y^{k+q+w}\\ &\left.\cdot G_{t+1,3t+1}^{3t,1}\left(\mathcal{D}y\middle|\begin{matrix}\Lambda_1\\ \Lambda_2\end{matrix}\right)dy\right]\\ =&\Gamma(m_D)\cdot\left\{\sum_{q=0}^{m_D-1}\frac{1}{q!}\left(\frac{m_D}{\overline{\gamma}_{RF,D}}\right)^q\sum_{w=0}^{\infty}\frac{1}{w!}\cdot(\Theta-1)^{k+q+w+1}\right.\\ &\cdot\left[-\left(\frac{m_E}{\overline{\gamma}_{RF,E}}+\frac{m_D}{\overline{\gamma}_{RF,D}}\right)\right]^w\\ &\cdot G_{t+2,3t+2}^{3t,2}\left(\mathcal{D}\cdot(\Theta-1)\middle|\begin{matrix}-(k+q+w),\Lambda_1\\ \Lambda_2,-(k+q+w+1)\end{matrix}\right)-\sum_{s=0}^{\infty}\frac{(\Theta-1)^{k+s+1}\left(-\frac{m_E}{\overline{\gamma}_{RF,E}}\right)^s}{s!}\\ &\left.\cdot G_{t+2,3t+2}^{3t,2}\left(\mathcal{D}\cdot(\Theta-1)\middle|\begin{matrix}-(k+s),\Lambda_1\\ \Lambda_2,-(k+s+1)\end{matrix}\right)\right\}.\end{aligned}\tag{37}$$

Finally, substituting the expressions of probabilities P_0, P_1, and P_2 into (29), the exact solution of the SOP for the investigated SC-based FSO/RF setup is obtained.

Remark 3. The probability of SPSC is another important performance metric, whose exact expression is evaluated directly by putting $R_s = 0$ or $\Theta = 1$ in corresponding SOP expression. ■

4.3. Asymptotic SOP analysis

In this subsection, we conduct the asymptotic SOP analysis under different conditions to gain in-depth understandings on the PLS performance of considered system.

4.3.1. $\mu_t \to \infty$

When $\mu_t \to \infty$ (i.e., $\mathcal{D} \to 0$) with limited SNRs for the RF links, the SC-based FSO/RF setup will employ the optical link for confidential information transmission while the radio channel will not be utilized. In this case, the SOP is actually equivalent to the COP with the expression given in (27). Then, by making use of asymptotic expression of G-function [5, Eq. (30)] in (27), we obtain the following asymptotic expression:

$$SOP^{\infty}\cong\mathcal{E}\cdot\frac{C}{\Gamma(m_D)}\cdot\hat{\Gamma}\left(m_D,\frac{m_D\cdot[\exp(R_s)-1]}{\overline{\gamma}_{RF,D}}\right)\cdot\left[\frac{(hab)^t}{\mu_t\,t^{2t}}\right]^{b_i},\tag{38}$$

where $\mathcal{E}=\sum_{i=1}^{3t}\frac{\prod_{j=1,j\neq i}^{3t}\Gamma(b_j-b_i)}{b_i\cdot\prod_{j=2}^{t+1}\Gamma(a_j-b_i)}$ and the parameters a_i and b_j represent the ith and jth terms of Λ_1 and Λ_2 respectively.

Recalling that the lowest power of μ_t dominates the asymptotic expression, it is concluded that as $\mu_t \to \infty$, the diversity order with respect to μ_t will be minimum of terms $\{\frac{c^2}{t},\frac{a}{t},\frac{b}{t}\}$.

Remark 4. The secrecy diversity of parallel FSO/RF setup under investigation relies largely upon the utilized FSO detection technique. More specifically, the diversity order for the configuration using IM/DD will only be half of that with the HD under the same FSO channel conditions. ■

Table 1
Simulation parameters of the optical fading link and RF amplifier.

Parameters of FSO links with varying turbulence severities [15]	
Strong atmospheric turbulence	$a = 2.064,\ b = 1.342$
Moderate atmospheric turbulence	$a = 2.296,\ b = 1.822$
Weak atmospheric turbulence	$a = 2.902,\ b = 2.51$
Parameters of PA with varying characteristics [21]	
Ideal PA	$\zeta = 1,\ \psi = 0$
Non-ideal PA	$P_{max} = 18$ dBm, $\psi = 0.5$

4.3.2. $\gamma_{RF,D} \to \infty$

In this case, the parallel FSO/RF communication system will always utilize radio channel for confidential information transmission, and the eavesdropper will also continuously intercept the information through the RF link. Therefore, the SOP under this scenario is equivalent to the probability P_2 with the expression given in (31). By utilizing the asymptotic property of lower incomplete Gamma function (i.e., $\lim_{x\to 0}\Gamma(a,x)\cong\frac{x^a}{a}$ [44, Eq. (06.06.06.0004.02)]), the asymptotic CDF $F_{\gamma_{sc}}^{\infty}$ as $\gamma_{RF,D}\to\infty$ is

$$F_{\gamma_{sc}}^{\infty}\cong\frac{C\cdot m_D^{m_D-1}}{\Gamma(m_D)\cdot\overline{\gamma}_{RF,D}^{m_D}}\cdot x^{m_D}\cdot G_{t+1,3t+1}^{3t,1}\left(\mathcal{D}\cdot x\middle|\begin{matrix}\Lambda_1\\ \Lambda_2\end{matrix}\right).\tag{39}$$

Substituting (3) and (39) into (31) and utilizing similar rationale as in (31)–(37) to derive P_2, the asymptotic SOP under the scenario $\gamma_{RF,D}\to\infty$ can be expressed by

$$\begin{aligned}SOP^{\infty}\cong&\frac{C\cdot m_D^{m_D-1}\cdot m_E^{m_E}\cdot\exp\left(\frac{m_E(\Theta-1)}{\Theta\cdot\overline{\gamma}_{RF,E}}\right)}{\Gamma(m_D)\Gamma(m_E)\cdot\overline{\gamma}_{RF,D}^{m_D}\overline{\gamma}_{RF,E}^{m_E}\cdot\Theta^{m_E}}\\ &\cdot\sum_{k=0}^{m_E-1}\binom{m_E-1}{k}(1-\Theta)^{m_E-1-k}\cdot\left[\mathcal{I}_c-\mathcal{I}_d\right],\end{aligned}\tag{40}$$

where

$$\mathcal{I}_c=\left(\frac{\overline{\gamma}_{RF,E}\Theta}{m_E}\right)^{m_D+k+1}\cdot G_{t+2,3t+1}^{3t,2}\left(\frac{\mathcal{D}\Theta\overline{\gamma}_{RF,E}}{m_E}\middle|\begin{matrix}-(m_D+k),\Lambda_1\\ \Lambda_2\end{matrix}\right),\tag{41}$$

$$\begin{aligned}\mathcal{I}_d=&\sum_{s=0}^{\infty}\frac{1}{s!}\cdot\left(-\frac{m_E}{\overline{\gamma}_{RF,E}\Theta}\right)^s\cdot(\Theta-1)^{m_D+k+s+1}\\ &\cdot G_{t+2,3t+2}^{3t,2}\left(\mathcal{D}\cdot(\Theta-1)\middle|\begin{matrix}-(m_D+k+s),\Lambda_1\\ \Lambda_2,-(m_D+k+s+1)\end{matrix}\right).\end{aligned}\tag{42}$$

Substituting (41) and (42) into (40), we obtain the asymptotic expression for SOP when $\gamma_{RF,D}\to\infty$. Noting that the diversity order is decided by the least exponent of $\gamma_{RF,D}$ in (40)–(42), it is obvious that the secrecy diversity order is m_D in terms of $\gamma_{RF,D}$.

Remark 5. If both $\gamma_{RF,D}$ and $\gamma_{RF,E}$ increase with the transmission power P_{RF} with the ratio $\frac{\overline{\gamma}_{RF,D}}{\overline{\gamma}_{RF,E}}$ being a constant, the diversity order when $P_{RF}\to\infty$ will be m_D+m_E with respect to the transmission power P_{RF}. ■

5. Simulation results and discussions

The PLS performance of the considered parallel communication setup having varying channel conditions is discussed in this section. The utilized simulation parameters for the FSO link fading and PA characteristics are given in Table 1. For the SOP analysis, we set the secrecy rate threshold as 0.5 nats per second per unit bandwidth.

Before elaborating on secrecy performance, we first examine the COP of parallel configuration versus that of single FSO system in Fig. 4, which shows the COP in terms of varying threshold SNRs for different link and hardware conditions. It is seen that the strong turbulence condition leads to poor FSO link connection, which is significantly enhanced using the parallel setup. Also, the non-ideal PA of

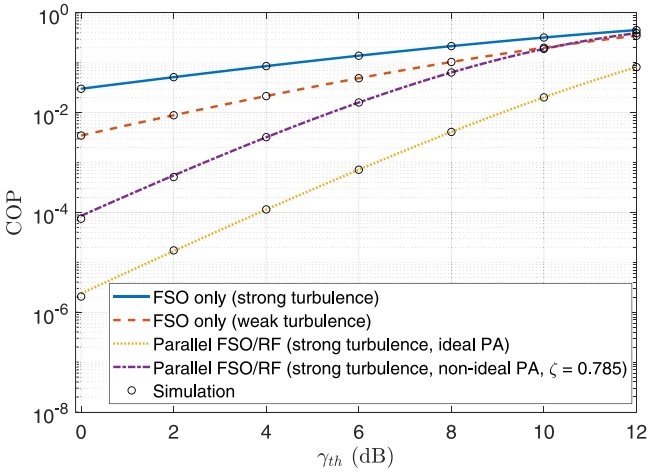

Fig. 4. The COP v.s. γ_{th} under the impact of FSO link turbulence and PA hardware efficiency (μ_1 = 15 dB, c = 6.7, P_{RF}^{cons} = 15 dBm, m_D = 3.2, Ω_D = 1).

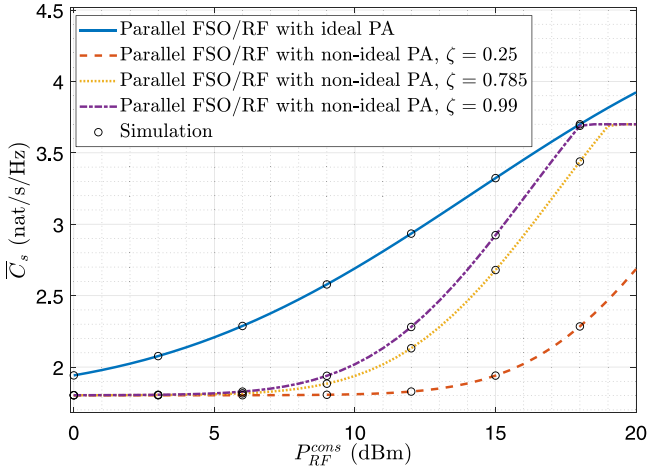

Fig. 5. The ASC v.s. P_{RF}^{cons} under the impact of PAs with varying levels of hardware efficiency (strong FSO turbulence, μ_2 = 5 dB, c = 1.0, m_D = 3, m_E = 2, Ω_D = 1, Ω_E = 0.01).

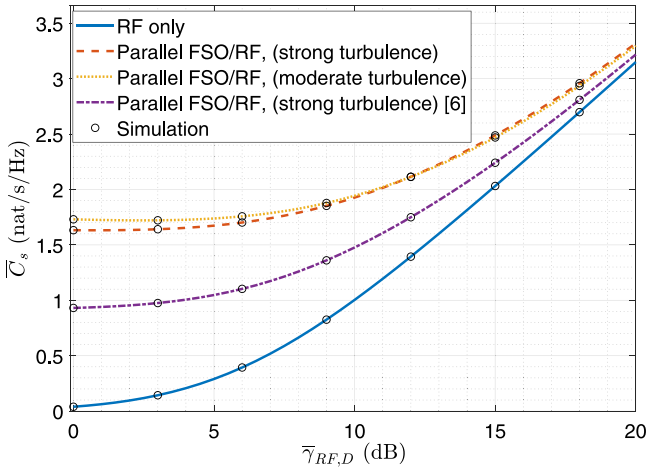

Fig. 6. The ASC v.s. $\overline{\gamma}_{RF,D}$ for the parallel FSO/RF setup under varying optical link conditions (μ_2 = 10 dB, c = 6.7, $\overline{\gamma}_{RF,E}$ = 5 dB, m_D = 3, m_E = 2).

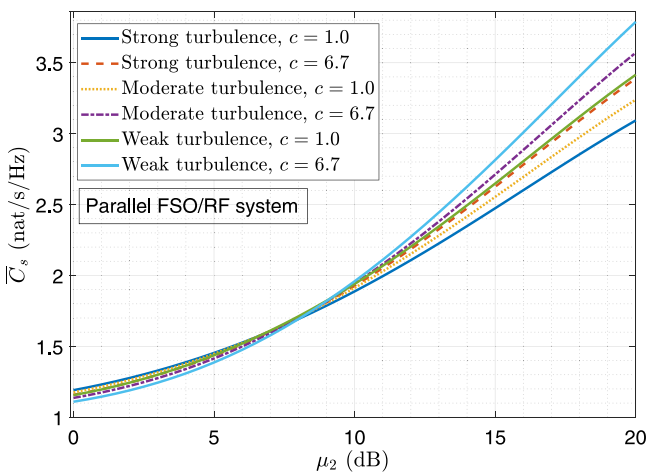

Fig. 7. The ASC versus μ_2 under varying FSO link conditions and FSO receiver pointing errors ($\overline{\gamma}_{RF,D}$ = 10 dB, $\overline{\gamma}_{RF,E}$ = 5 dB, m_D = 3, m_E = 2).

the RF sub-system of the hybrid system largely degrades the connection performance compared to that with ideal PA.

5.1. ASC performance

Fig. 5 illustrates how PA nonideality affects ASC of the investigated parallel setup. It can be seen that the ASC for the case with ideal PA appears as an upper limit compared to the cases with imperfect PAs. This is due to the fact that the secrecy capacity depends on the ergodic capacity difference between the legitimate and eavesdropping transmissions. When the transmitted power of RF link (i.e., the output power of PA) increases, the ergodic capacities of both transmissions will increase. However, the increase for the legitimate transmission appears to be larger than that of the eavesdropping link due to the diversity transmission of the legitimate transmission. This implies that as the output power of the PA increases, the ASC will also increase. Since with the same PA input power, the output power for ideal PA will always be larger than that from the imperfect PA, thus leading to the fact that the ASC will be larger in the former case than the latter with the same input power of PA P_{RF}^{cons}. In other words, the ASC for the case with ideal PA appears as an upper bound compared to the cases with imperfect PAs. It is also observed that the PA inefficiency exhibits a significantly adverse impact on the system's secrecy. Resulting from the characteristics of imperfect PA as shown in Fig. 2 (i.e., the efficiency of any imperfect PA becomes lower when the consumed power of the PA is smaller), the ASC stays stagnant when P_{RF}^{cons} is small that leads to even smaller output power P_{RF} due to further impairment from the imperfect PA (as can be seen in Fig. 3). After the consumed power of PA P_{RF}^{cons} grows to some threshold and the PA's output power limit (i.e., P_{RF}^{max}) is reached, further increasing the consumed power of the PA does not change the output power of the PA P_{RF}, which thus results in a stagnant ASC again.

In Fig. 6, ASC of investigated parallel FSO/RF setup is plotted against average SNR of legitimate radio communication link. It is seen the investigated parallel setup has much improved ASC compared to RF-only system even when optical communication link undergoes strong turbulent situations. As another point of view, the inclusion of the radio communication link into the parallel system makes the system more robust to the FSO turbulence.

In Fig. 7, the impacts of optical link turbulence and receiver misalignment on ASC are depicted. It is observed that both FSO receiver misalignment and turbulence have adverse effects on the ASC performance, and they exhibit greater impact on the ASC performance as the optical link quality becomes better. However, it can also be seen from Fig. 7 that the atmospheric turbulence poses less performance variation on the ASC for the parallel RF-FSO system compared to the FSO-only or cascaded RF/FSO system in [5,15]. Moreover, intersection between the

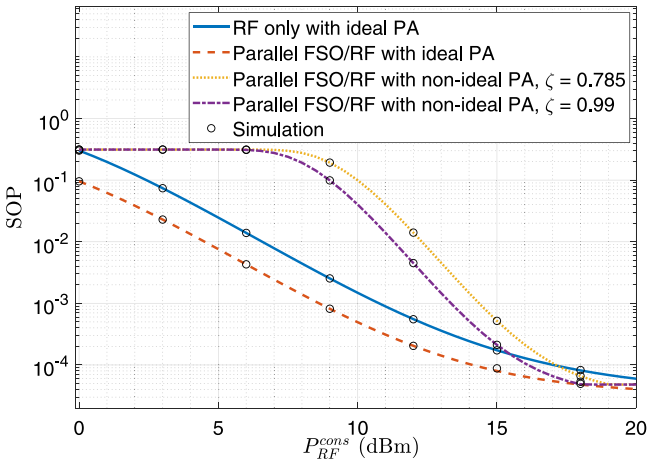

Fig. 8. The SOP versus P_{RF}^{cons} under the impact of PAs with different levels of hardware efficiency (weak FSO turbulence, $\mu_2 = 5$ dB, $c = 6.7$, $m_D = 3$, $m_E = 2$, $\Omega_D = 1$, $\Omega_E = 0.01$).

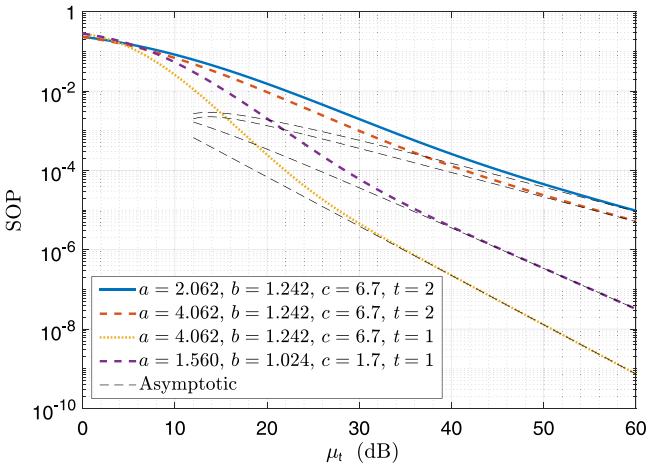

Fig. 10. The SOP versus μ_t for various FSO turbulence scenarios and FSO detection techniques ($\overline{\gamma}_{RF,D} = 5$ dB, $\overline{\gamma}_{RF,E} = 5$ dB, $m_D = 3.2$, $m_E = 2$).

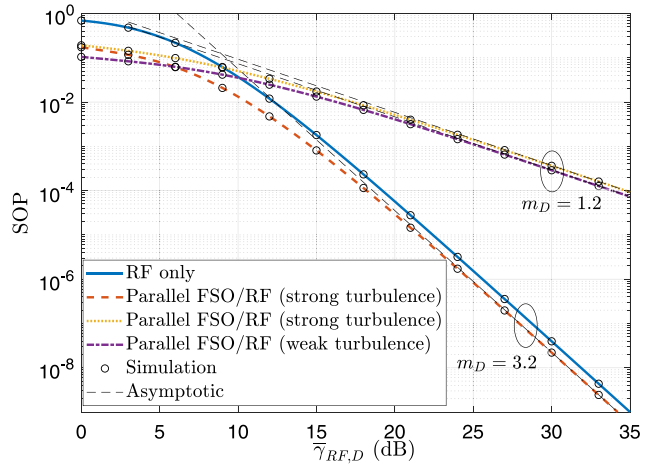

Fig. 9. The SOP versus $\overline{\gamma}_{RF,D}$ for the parallel FSO/RF setup under varying optical link conditions ($\overline{\gamma}_{RF,E} = 0$ dB, $m_E = 2$, $c = 6.7$, and $\mu_2 = 10$ dB).

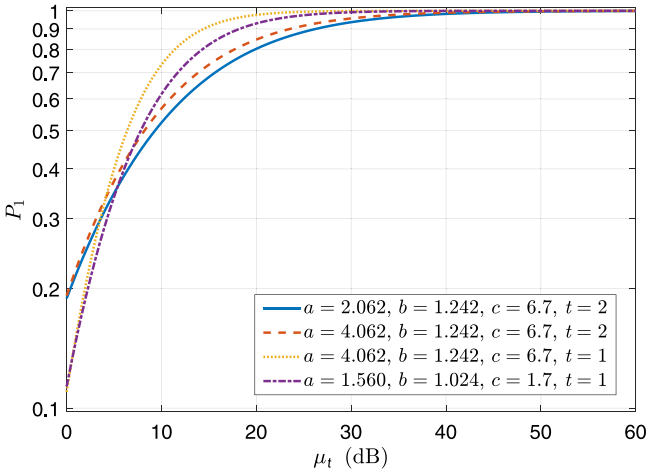

Fig. 11. The probability P_1 versus μ_t under varying FSO turbulence and FSO detection techniques ($\overline{\gamma}_{RF,D} = 5$ dB, $\overline{\gamma}_{RF,E} = 5$ dB, $m_D = 3.2$, $m_E = 2$).

curves corresponding to varying turbulence is found in Fig. 7. It occurs because when the optical SNR μ_2 is below some threshold, the hybrid system with more severe turbulence will have slightly higher capacity. While the opposite trend is true when the optical SNR is large enough. This intersection of the ergodic capacity of the legitimate transmission translates to the intersection of the ASC curves with the RF power being unchanged. The similar intersection for curves of ergodic capacity v.s. optical SNR under varying turbulence levels has also been reported for the parallel RF/FSO system with selection combining in [48, Fig. 3]. It can also be observed from Fig. 7 that the ASC variations due to the pointing errors caused by jitter are much less before the aforementioned intersection due to the small values of the ASCs when the optical SNR μ_2 is below the threshold corresponding to the intersection.

5.2. SOP performance

The effects of PA nonideality on SOP are depicted in Fig. 8. It can be observed that the SOP for the case with ideal PA is the lower limit compared to the cases with imperfect PAs due to the same reason as analyzed for the ASC in Fig. 5. For non-ideal PA, the SOP will stay stagnant when the consumed power P_{RF}^{cons} is small. This is because the output power of the PA P_{RF} is too small due to low consumed power and low PA efficiency as can be seen in Figs. 2 and 3, which makes the RF SNRs still worse compared to the optical communication link; thus, the SOP performance is still dominated by the FSO communication link quality. It is also observed that the SOP will stay stagnant again when the consumed power P_{RF}^{cons} is larger than some threshold. This is because the maximum output power of the imperfect PA has reached and further increasing the input power of imperfect PA cannot further improve the transmission power of the PA, thus resulting in a stagnant SOP again.

In Fig. 9, SOP of the investigated parallel FSO/RF setup is plotted against average SNR of the legitimate radio link. The results in Fig. 9 again demonstrate the improved secrecy of the proposed SC-based parallel setup in this paper compared to the isolated RF system. For the analytical curve corresponding to strong turbulence with $m_D = 3.2$, the SOP at the SNR $\gamma_{RF,D}$ of 35 dB and 25 dB are $5.595 \cdot 10^{-10}$ and $8.401 \cdot 10^{-7}$, respectively. Then, the slope of the curve is calculated as $\log_{10}\left(\frac{8.401 \cdot 10^{-7}}{5.595 \cdot 10^{-10}}\right) = 3.1765 \approx m_D = 3.2$, thus validating the asymptotic analysis in Section 4.3.2. Therefore, the asymptotic analysis on the SOP for the scenario of $\gamma_{RF,D} \to \infty$ in Section 4.3 is validated from Fig. 9.

The SOP of the hybrid system under varying turbulence conditions and detection techniques is plotted in terms of optical communication link's SNR in Fig. 10. Clearly, the FSO receiver detection type has a large impact on the SOP. Additionally, when the optical link's SNR is

smaller than some threshold value, the hybrid system with the FSO sub-system employing HD ($t = 1$) has superior SOP performance than that with IM/DD ($t = 2$). Instead, when the optical link quality is above some level, the system with IM/DD technique exhibits better performance than that with HD technique in terms of SOP. This is related to the statistics of the instantaneous SNR for the FSO receiver with different detection types. As the optical SNR μ_t is lower than some threshold, the probability of the SC-based setup using FSO signals for demodulation (namely the probability P_1) is larger when the FSO system is equipped with IM/DD technique compared to the case using HD technique; and the opposite trend holds when the electrical SNR is larger than the threshold. This is verified numerically by the plot of probability P_1 in Fig. 11, where an interaction is observed between the curves corresponding to IM/DD and HD detections due to the above reasons.

Furthermore, we observe from Fig. 10 that for the dashed curve ($a = 1.560$, $b = 1.024$, $c = 1.7$, and $t = 1$), the SOPs at the SNR μ_1 of 60 dB and 59 dB are $3.211 \cdot 10^{-8}$ and $4.064 \cdot 10^{-8}$, respectively. Then, the slope of the curve at high-SNR is calculated as $10 \cdot \log_{10}\left(\frac{4.064 \cdot 10^{-8}}{3.211 \cdot 10^{-8}}\right) = 1.0231 \approx \min\{\frac{c^2}{t}, \frac{a}{t}, \frac{b}{t}\} = 1.024$. For the solid curve ($a = 2.062$, $b = 1.242$, $c = 6.7$, and $t = 2$), the SOPs at the SNR μ_2 of 60 dB and 59 dB are $9.628 \cdot 10^{-6}$ and $1.117 \cdot 10^{-5}$, respectively. Then, the slope of the curve at high-SNR is calculated as $10 \cdot \log_{10}\left(\frac{4.484 \cdot 10^{-5}}{9.628 \cdot 10^{-6}}\right) = 0.6452 \approx \min\{\frac{c^2}{t}, \frac{a}{t}, \frac{b}{t}\} = 0.6210$. Hence, the asymptotic analysis performed in Section 4.3.1 for the case of $\mu_r \to \infty$ is validated.

6. Summary and conclusions

The PLS performance analysis of a parallel optical and RF setup with SC was conducted in this paper. Exact closed-form expressions for performance indicators such as connection outage probability, average secrecy capacity, and secrecy outage probability were derived by including the effects of FSO channel atmospheric turbulence and RF hardware nonideality. Furthermore, the secrecy diversity analysis was also performed to obtain in-depth understandings into the PLS performance of the investigated parallel setup. The results show that the FSO turbulence and the RF PA inefficiency largely affect the connectivity of the investigated parallel system. Meanwhile, the investigated SC-based parallel system is more robust than the FSO-only system in connectivity and is superior to the isolated RF system in secrecy performance.

Declaration of competing interest

The authors declare that they have no known competing financial interests or personal relationships that could have appeared to influence the work reported in this paper.

Acknowledgments

The work of Y. Ai and M. Cheffena was supported by the Norwegian University of Science and Technology (NTNU), Norway. The work of H. Lei was supported by the National Natural Science Foundation of China under Grant 61971080 and the Opend Fund of the Shannxi Key Laboratory of Information Communication Network and Security under Grant ICNS201807.

References

[1] M. Alzenad, M.Z. Shakir, H. Yanikomeroglu, M.-S. Alouini, FSO-based vertical backhaul/fronthaul framework for 5G+ wireless networks, IEEE Commun. Mag. 56 (1) (2018) 218–224.

[2] E. Zedini, I.S. Ansari, M.-S. Alouini, Performance analysis of mixed Nakagami-m and Gamma-Gamma dual-hop FSO transmission systems, IEEE Photonics J. 7 (1) (2015) 1–20.

[3] fSONA Communications, Security of a free space optical transmission, 2019, http://www.fsona.com/tech/app_notes/fSONA-APPNOTE-FSO_Security.pdf. (Online; Accessed 20 June 2019).

[4] CableFree, FSO Guide – Free space optics, Optical wireless, 2019, https://www.cablefree.net/wirelesstechnology/free-space-optics/fso-guide/. (Online; Accessed 20 June 2019).

[5] Y. Ai, A. Mathur, M. Cheffena, M. Bhatnagar, H. Lei, Physical layer security of hybrid satellite-FSO cooperative systems, IEEE Photonics J. 11 (1) (2019) 1–14.

[6] W.M.R. Shakir, Performance evaluation of a selection combining scheme for the hybrid FSO/RF system, IEEE Photonics J. 10 (1) (2018) 1–10.

[7] M. Usman, H.-C. Yang, M.-S. Alouini, Practical switching-based hybrid FSO/RF transmission and its performance analysis, IEEE Photonics J. 6 (5) (2014) 1–13.

[8] T. Rakia, H.-C. Yang, M.-S. Alouini, F. Gebali, Outage analysis of practical FSO/RF hybrid system with adaptive combining, IEEE Commun. Lett. 19 (8) (2015) 1366–1369.

[9] A. Touati, A. Abdaoui, F. Touati, M. Uysal, A. Bouallegue, On the effects of combined atmospheric fading and misalignment on the hybrid FSO/RF transmission, IEEE/OSA J. Opt. Commun. Networking 8 (10) (2016) 715–725.

[10] N. Letzepis, K.D. Nguyen, A.G. i Fàbregas, W.G. Cowley, Outage analysis of the hybrid free-space optical and radio-frequency channel, IEEE J. Sel. Areas Commun. 27 (9) (2009) 1709–1719.

[11] V. Jamali, D.S. Michalopoulos, M. Uysal, R. Schober, Mixed RF and hybrid RF/FSO relaying, in: Proceedings of IEEE Global Communications Conference Workshop, GC Wkshps, IEEE, San Diego, CA, USA, 2015, pp. 1–6.

[12] B. Makki, T. Svensson, T. Eriksson, M.-S. Alouini, Performance analysis of ARQ-based RF-FSO links, IEEE Commun. Lett. 21 (6) (2017) 1253–1256.

[13] H. Lei, Z. Dai, K.-H. Park, W. Lei, G. Pan, M.-S. Alouini, Secrecy outage analysis of mixed RF-FSO downlink SWIPT systems, IEEE Trans. Commun. 66 (12) (2018) 6384–6395.

[14] H. Lei, H. Luo, K.-H. Park, Z. Ren, G. Pan, M.-S. Alouini, Secrecy outage analysis of mixed RF-FSO systems with channel imperfection, IEEE Photonics J. 10 (3) (2018) 1–13.

[15] H. Lei, Z. Dai, I.S. Ansari, K.-H. Park, G. Pan, M.-S. Alouini, On secrecy performance of mixed RF-FSO systems, IEEE Photonics J. 9 (4) (2017) 1–14.

[16] L. Yang, T. Liu, J. Chen, M.-S. Alouini, Physical-layer security for mixed η–μ and $\mathcal{M}$-distribution dual-hop RF/FSO systems, IEEE Trans. Veh. Technol. 67 (12) (2018) 12427–12431.

[17] A.H.A. El-Malek, A.M. Salhab, S.A. Zummo, M.-S. Alouini, Security-reliability trade-off analysis for multiuser SIMO mixed RF/FSO relay networks with opportunistic user scheduling, IEEE Trans. Wireless Commun. 15 (9) (2016) 5904–5918.

[18] A.H.A. El-Malek, A.M. Salhab, S.A. Zummo, M.-S. Alouini, Effect of RF interference on the security-reliability tradeoff analysis of multiuser mixed RF/FSO relay networks with power allocation, J. Lightwave Technol. 35 (9) (2017) 1490–1505.

[19] Y. Wu, A. Khisti, C. Xiao, G. Caire, K.-K. Wong, X. Gao, A survey of physical layer security techniques for 5G wireless networks and challenges ahead, IEEE J. Sel. Areas Commun. 36 (4) (2018) 679–695.

[20] M. Bloch, J. Barros, M.R. Rodrigues, S.W. McLaughlin, Wireless information-theoretic security, IEEE Trans. Inform. Theory 54 (6) (2008) 2515–2534.

[21] B. Makki, T. Svensson, T. Eriksson, M. Nasiri-Kenari, On the throughput and outage probability of multi-relay networks with imperfect power amplifiers, IEEE Trans. Wirel. Commun. 14 (9) (2015) 4994–5008.

[22] I.S. Gradshteyn, I.M. Ryzhik, Table of Integrals, Series, and Products, seventh ed., Academic Press, Burlington, MA, USA, 2007.

[23] A. Mathur, M.R. Bhatnagar, Y. Ai, M. Cheffena, Performance analysis of a dual-hop wireless-power line mixed cooperative system, IEEE Access 6 (2018) 34380–34392.

[24] S. Panic, M. Stefanovic, J. Anastasov, P. Spalevic, Fading and Interference Mitigation in Wireless Communications, CRC press, New York, NY, USA, 2013.

[25] R. Vaughan, J.B. Andersen, Channels, Propagation and Antennas for Mobile Communications, Vol. 50, IET, Herts, UK, 2003.

[26] E. Zedini, H. Soury, M.-S. Alouini, On the performance analysis of dual-hop mixed FSO/RF systems, IEEE Trans. Wirel. Commun. 15 (5) (2016) 3679–3689.

[27] I.S. Ansari, F. Yilmaz, M.-S. Alouini, Performance analysis of FSO links over unified Gamma-Gamma turbulence channels, in: Proceedings of IEEE Vehicular Technology Conference, VTC–Spring, IEEE, Glasgow, UK, 2015, pp. 1–5.

[28] A. Jurado-Navas, J.M. Garrido-Balsells, J.F. Paris, A. Puerta-Notario, J. Awrejcewicz, A unifying statistical model for atmospheric optical scintillation, Numer. Simulat. Phys. Eng. Process. 181 (8) (2011) 181–205.

[29] Y. Ai, M. Cheffena, On multi-hop decode-and-forward cooperative relaying for industrial wireless sensor networks, Sensors 17 (4) (2017) 695.

[30] A.H.A. El-Malek, M.A. Aboulhassan, A.M. Salhab, S.A. Zummo, Performance analysis and power optimization for spectrum-sharing mixed RF/FSO relay networks with energy harvesting, IEEE Photonics J. 11 (2) (2019) 1–17.

[31] B. Makki, T. Svensson, M. Brandt-Pearce, M.-S. Alouini, On the performance of millimeter wave-based RF-FSO multi-hop and mesh networks, IEEE Trans. Wireless Commun. 16 (12) (2017) 7746–7759.

[32] D. Persson, T. Eriksson, E.G. Larsson, Amplifier-aware multiple-input single-output capacity, IEEE Trans. Commun. 62 (3) (2014) 913–919.

[33] D. Persson, T. Eriksson, E.G. Larsson, Amplifier-aware multiple-input multiple-output power allocation, IEEE Commun. Lett. 17 (6) (2013) 1112–1115.

[34] H.M. Nemati, C. Fager, H. Zirath, High efficiency LDMOS current mode class-D power amplifier at 1 GHz, in: Proceedings of European Microwave Conference, EuMC, IEEE, Manchester, UK, 2006, pp. 176–179.

[35] M.K. Simon, M.-S. Alouini, Digital Dommunication over Fading Channels, Vol. 95, John Wiley & Sons, New York, NY, USA, 2005.
[36] Y. Ai, M. Cheffena, A. Mathur, H. Lei, On physical layer security of double Rayleigh fading channels for vehicular communications, IEEE Wirel. Commun. Lett. 7 (6) (2018) 1038–1041.
[37] Y. Ai, M. Cheffena, T. Ohtsuki, H. Zhuang, Secrecy performance analysis of wireless sensor networks, IEEE Sens. Lett. 3 (5) (2019) 4.
[38] A. Prudnikov, Y. Brychkov, O. Marichev, Integrals and Series. Vol. 3: More Special Functions, Gordon and Breach Sci. Publ., New York, NY, USA, 1986.
[39] Y. Ai, A. Mathur, L. Kong, M. Cheffena, Effective throughput analysis of α-η-κ-μ fading channels, IEEE Access 8 (2020) 57363–57371.
[40] P. Mittal, K. Gupta, An integral involving generalized function of two variables, Proc. Indian Acad. Sci. A 75 (3) (1972) 117–123.
[41] H. Lei, I.S. Ansari, G. Pan, B. Alomair, M.-S. Alouini, Secrecy capacity analysis over α-μ fading channels, IEEE Commun. Lett. 21 (6) (2017) 1445–1448.
[42] K.P. Peppas, A new formula for the average bit error probability of dual-hop amplify-and-forward relaying systems over generalized shadowed fading channels, IEEE Wirel. Commun. Lett. 1 (2) (2012) 85–88.
[43] V. Adamchik, O. Marichev, The algorithm for calculating integrals of hypergeometric type functions and its realization in REDUCE system, in: Proceedings of International Symposium on Symbolic and Algebraic Computation, ISSAC, ACM, Tokyo, Japan, 1990, pp. 212–224.
[44] The wolfram functions site, 2019, URL http://functions.wolfram.com/. (Accessed 2 January 2019).
[45] S. Vuppala, Y.J. Tolossa, G. Kaddoum, G. Abreu, On the physical layer security analysis of hybrid millimeter wave networks, IEEE Trans. Commun. 66 (3) (2018) 1139–1152.
[46] L. Kong, Y. Ai, J. He, N. Rajatheva, G. Kaddoum, Intercept probability analysis over the Cascaded Fisher–Snedecor $\mathcal{F}$ fading wiretap channels, in: Proceedings of International Symposium on Wireless Communication Systems, ISWCS, IEEE, Oulu, Finland, 2019, pp. 672–676.
[47] Y. Ai, L. Kong, M. Cheffena, Secrecy outage analysis of double shadowed Rician channels, Electron. Lett. 55 (13) (2019) 765–767.
[48] H. Liang, C. Gao, Y. Li, M. Miao, X. Li, Analysis of selection combining scheme for hybrid FSO/RF transmission considering misalignment, Opt. Commun. 435 (2019) 399–404.